ELSEVIER

PII: S0032-3861(97)00177-8

Polymer Vol. 38 No. 25, pp. 6189–6195, 1997

0032-3861/97/$17.00+0.00

An investigation of the high molecular weight poly(ethylene oxide)–zinc bromide complexes

Sangamithra Chintapalli and Roger Frech*
Department of Chemistry and Biochemistry, The University of Oklahoma, Norman, OK 73019, USA

and Brian Grady
Department of Chemical Engineering and Material Science, The University of Oklahoma, Norman, OK 73019, USA
(Received 17 June 1996)

Structural characterization studies using Raman and i.r. spectroscopy and extended X-ray absorption fine structure (EXAFS) on the $(PEO)_n[(ZnBr_2)_{1-x}(LiBr)_x]$ system ($n = 20$, 40; $x = 0$–0.8) are reported. Raman spectroscopy reveals that the ionic species present in the complex depend on the Zn : Li ratio and the ether oxygen to metal ion ratio. With increasing x values, the species vary from $ZnBr_2$ to $ZnBr_3^-$ to $ZnBr_4^{2-}$. EXAFS measurements confirm that the Zn–Br coordination number is higher for the $(PEO)_n[(ZnBr_2)_{1-x}(LiBr)_x]$ system than the $(PEO)_nZnBr_2$ system. In the $(PEO)_{20}$ $[(ZnBr_2)_{0.2}(LiBr)_{0.8}]$ composition, no oxygen neighbours of zinc are apparent while a significant Zn–O contribution is present in the $(PEO)_{40}[(ZnBr_2)_{0.6}(LiBr)_{0.4}]$ and $(PEO)_{40}ZnBr_2$ complexes. Temperature dependent EXAFS measurements of $(PEO)_{20}$ $[(ZnBr_2)_{0.2}(LiBr)_{0.8}]$ show that ionic association is not altered with lowering of temperature. The effect of addition of tetraethylene glycol (TEG) and its dimethyl ether (TEGDME) to the complex is also reported. © 1997 Elsevier Science Ltd.

(Keywords: polymer electrolyte; EXAFS; Raman)

INTRODUCTION

The wide range of technological applications of solid polymer electrolytes[1–6] has spurred attempts to understand fast ion-transport in polymer systems. The polymer electrolyte materials are characterized by an interesting conductivity behaviour that is highly dependent on local structure and is influenced by crystallization and ionic association. At temperatures below ~65°C, PEO–salt electrolytes consist of mixtures of spherulitic crystalline regions separated by amorphous solutions of salt in PEO; ion conduction occurs primarily in the amorphous regions[7–9]. One of the methods to improve the conductivity of PEO-based electrolytes include modification of the polymer matrix by incorporation of plasticizers to make the matrix more liquid-like. Addition of small molecules such as ethylene carbonate, propylene carbonate and PEO oligomers as plasticizers facilitate long chain segmental motion. A serious disadvantage, however, is that most plasticizers are volatile at room temperature leading to their loss from the samples.

To completely understand the mechanism of ionic transport in polymer electrolytes, the morphological structure must be fully characterized. In this paper, the local structure around the ionic species is characterized using EXAFS which is an averaging technique and gives information such as coordination number and distance of neighbours around an absorbing atom. A theoretical description of EXAFS is found elsewhere[10]. Additional local structural information can be provided by Raman spectroscopy which can help ascertain the different ionic species present in the salt complexes.

Several PEO–zinc salt complexes have been characterized by optical microscopy, d.s.c., EXAFS, conductance measurements, and transport number determinations[11–23]. In this paper, results of Raman i.r. and EXAFS studies of the PEO–($ZnBr_2$ + LiBr) systems are presented. The effect of plasticizer addition will also be discussed.

EXPERIMENTAL

PEO (MW 4×10^6, Aldrich, Milwaukee, WI, USA) was used as received. $ZnBr_2$ (Aldrich) and LiBr (Aldrich) were dried in a vacuum oven at 100°C for 48 h. Tetraethylene glycol (Aldrich) was vacuum-distilled over dry molecular sieves and tetraethylene glycol dimethyl ether (Aldrich) was vacuum distilled over dry CaH_2 at 120°C. Stoichiometric amounts of PEO, plasticizer and salt were dissolved in acetonitrile and stirred at room temperature for 24 h. Thin films were cast on Teflon sheets by the slow-evaporation of solvent. The films were dried at room temperature for 24 h and then dried in a vacuum oven at ~50°C for another 24 h.

* To whom correspondence should be addressed

Room temperature Raman spectra were recorded using a Jobin Yvon T64000 Raman system. Spectra were recorded with the triple monochromator at a 16 s integration time using 10 accumulations. The argon ion laser line at 514.5 nm was used at a power of 300 mW.

I.r. spectra were recorded using Digilab FTS-40 Bio-Rad i.r. spectrometer in the region 4000–400 cm^{-1} at a resolution of 2 cm^{-1}. For i.r. studies, the polymer–salt complexes were cast on 38 mm × 19 mm × 4 mm CsI windows and dried at ~100°C for 20–30 min to ensure solvent evaporation.

Thin film samples for EXAFS were prepared such that $\mu t \sim 2$ at 100 eV above the K-edge of the neutralizing cation where t is the sample thickness and μ is the absorption coefficient. K-edge EXAFS spectra were collected at the Stanford Synchrotron Radiation Laboratory on Beamline 2–3. For these samples, 5 eV steps were used in the pre-edge region and EXAFS region, while 2 eV steps were employed from 13 eV below the edge to 41 eV above the edge. Entrance slits of 0.7 mm were used to obtain high-energy resolution. Energy calibration was performed with pure zinc metal foil. Two ionization chambers, one of 15 cm length and the other of 30 cm length, filled with N_2 were used to monitor the incoming and outgoing intensities of X-rays respectively. A total of five scans (each scan lasted approximately 15 min) were collected and the scans were averaged after E_0 determination to improve the signal to noise ratio. The samples were mounted in a special sample holder and purged with nitrogen gas during measurement.

After isolation of the EXAFS oscillations, the data were Fourier transformed to obtain the radial structure function (RSF) which is similar to a radial distribution function. Locations of the peaks are shifted from the real interatomic distances; hence, a subscript F will be used to distinguish RSF distances from the actual distance R. A commercial software package, Autobk, available from the University of Washington UWXAFS project, was used for the conversion of the measured μt vs. E curve to $k\chi(k)$ vs. k where E is the energy and k is the wave vector. No standard was used in the background subtraction. All simulations were also weighted by k^1 in order to facilitate direct comparison between the simulated and experimental curves. FEFFIT and FEFF6[24], both from UWAXS, were used to fit the experimental data to theoretical data for the range $R_F = 1.25–3$ assuming a combination of oxygen and bromine neighbours in the first shell. The data were truncated at $k = 12.5$ due to the presence of a crystal glitch at $k \sim 12.8$. E_0 was varied in order to compensate for errors involving energy calibration and phase-transferability[27]. The amplitude reduction factor (S_0^2) was held constant at 0.9. This value was determined after allowing S_0^2 to vary during initial fitting. The Zn–Br coordination number was set from curve-fitting results of the Raman data and these are shown in *Table 2*. Therefore four adjustable parameters were used in the fitting of experimental data to theory: the Debye–Waller factors for the Zn–Br and Zn–O coordination shell respectively, the edge-energy and Zn–O coordination number. The shifts in the edge-energy ranged from 1 to 3 eV.

A cryogenic sample holder was used for the EXAFS measurements at 5.5 K, 20 K, 60 K, 120 K and 200 K. Liquid helium was used for cooling. The sample was kept at each temperature for 15 min before measurement. For temperatures below 100 K, helium gas was used as the purge gas while nitrogen was used for the higher temperatures.

RESULTS AND DISCUSSION

Raman spectroscopy

The Raman spectra of $(PEO)_{20}ZnBr_2$, $(PEO)_{20}[(ZnBr_2)_{0.5}(LiBr)_{0.5}]$ and $(PEO)_{20}[(ZnBr_2)_{0.2}(LiBr)_{0.8}]$ in the region 250–140 cm^{-1} are shown in *Figure 1*. $(PEO)_{20}[(ZnBr_2)_{0.5}(LiBr)_{0.5}]$ (curve labelled 1 : 1) shows two peaks at 179 and 164 cm^{-1} which have been assigned to the symmetric stretching mode (ν_s) of $ZnBr_3^-$ and $ZnBr_4^{2-}$ respectively and are consistent with earlier studies[23,26–28]. These spectra are similar to those observed in $(PEO)_{20}[(ZnBr_2)_{0.5}(LiBr)_{0.5}]$[23]. In $(TEG)_{20}[(ZnBr_2)_{0.5}(LiBr)_{0.5}]$ and $(TEGDME)_{20}[(ZnBr_2)_{0.5}(LiBr)_{0.5}]$, the only species is $ZnBr_3^-$. The Raman spectra of $(PEO)_n[(ZnBr_2)_{0.2}(LiBr)_{0.8}]$ ($n = 5$, 10, 20) only show $ZnBr_4^{2-}$ species (curve labelled 1 : 4) as observed in $(PPO)_{20}[(ZnBr_2)_{0.2}(LiBr_{0.8}]$ and $(TEGDME)_{20}[(ZnBr_2)_{0.2}(LiBr)_{0.8}]$. However in $(TEG)_{20}[(ZnBr_2)_{0.2}(LiBr)_{0.8}]$ a mixture of $ZnBr_3^-$ and $ZnBr_4^{2-}$ is seen, with the former species predominant. In $(PEO)_{20}ZnBr_2$ a mixture of $ZnBr_2$ and $ZnBr_3^-$ are observed (curve labelled 1 : 0).

The relative intensities of the different zinc bromide species in the polymer complexes were obtained by curve-fitting the bands in the Raman spectra to a straight base line and one Gaussian–Lorentzian product function for each band using a non-linear least-squares method (Grams 386®, Galactic Industries). *Table 1* summarizes the results of the curve-fitting data for $(PEO)_n[(ZnBr_2)_{1-x}(LiBr)_x]$ complexes. Curve fitting results in the TEG, TEGDME and PPO salt complexes are also included for comparison. The results show that

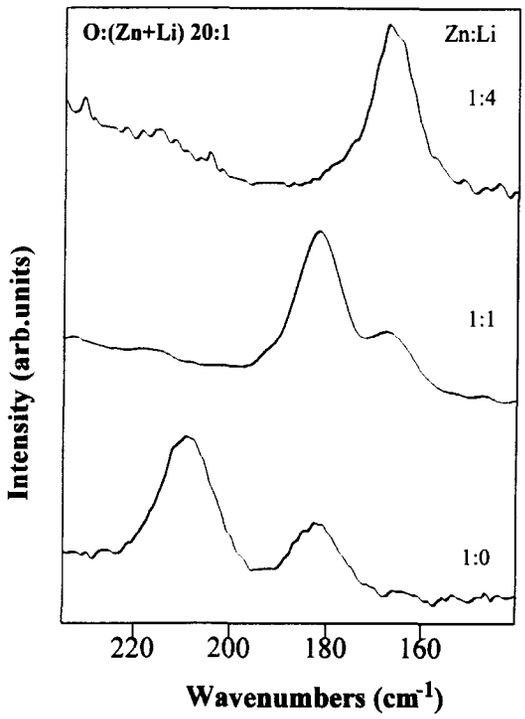

Figure 1 Raman spectra of $(PEO)_{20}[(ZnBr_2)_{1-x}(LiBr)_x]$, $x = 0.2$, 0.5, 1.0, complexes in the region 250–140 cm^{-1}

Table 1 Results of curve-fitting in the 250–150 cm^{-1} region for different polymer–zinc bromide complexes

Composition	Relative intensities		
	$ZnBr_2$	$ZnBr_3^-$	$ZnBr_4^{2-}$
$(PPO)_{20}[(ZnBr_2)_{0.5}(LiBr)_{0.5}]$	–	90.0	10.0
$(TEG)_{20}[(ZnBr_2)_{0.5}(LiBr)_{0.5}]$	–	100.0	–
$(TEGDME)_{20}[(ZnBr_2)_{0.5}(LiBr)_{0.5}]$	–	100.0	–
$(PEO)_{20}[(ZnBr_2)_{0.5}(LiBr)_{0.5}]$	–	74.0	26.0
$(PEO)_5[(ZnBr_2)_{0.6}(LiBr)_{0.4}]$	–	63.2	36.8
$(PEO)_{40}[(ZnBr_2)_{0.6}(LiBr)_{0.4}]$	–	89.8	10.2
$(PEO)_5[(ZnBr_2)_{0.5}(LiBr)_{0.5}]$	–	27.7	72.3
$(PEO)_{30}ZnBr_2$	81.0	19.0	–
$(PEO)_{20}ZnBr_2$	74.0	26.0	–

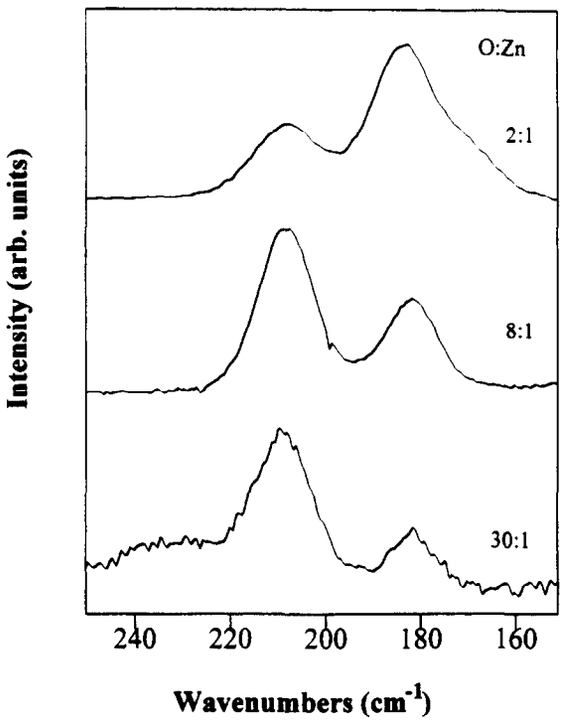

Figure 2 Raman spectra of $(PEO)_nZnBr_2$ complexes as a function of O : M ratio in the spectral region 250–140 cm^{-1}

TEGDME and PEO exhibit very similar behaviour towards cation coordination as reported earlier[29]. Also, PPO and PEO behave similarly owing to their long-chain length. The small differences may be related to their differing abilities to coordinate cations.

Increasing the salt concentration (decreasing n), with the Zn : Li ratio constant, in the $(PEO)_n[(ZnBr_2)_{0.2}(LiBr)_{0.8}]$ complex does not change the relative amounts of ionic species present; this observation suggests that $ZnBr_4^{2-}$ is favoured greatly at this Zn : Li ratio. Keeping the ether oxygen to total metal (Zn + Li) ratio constant and decreasing x does change the speciation. When a mixture of species are present for a given x value ($x = 0$–0.7), decreasing n also changes the speciation. For the $(PEO)_n[(ZnBr_2)_{0.6}(LiBr)_{0.4}]$ complex, decreasing n from 40 to 5 increases the intensity of $ZnBr_4^{2-}$ species relative to $ZnBr_3^-$ species. The Raman spectra of $(PEO)_nZnBr_2$ complexes ($n = 200$ to 2) show that with increasing salt concentration (decreasing n) the salt complexes shift from pure $ZnBr_2$ species to a mixture of $ZnBr_2$ and $ZnBr_3^-$ species. *Figure 2* shows the speciation in the Raman spectral region 250–140 cm^{-1} for three different compositions.

Raman studies of zinc bromide complexes in poly(propylene oxide), poly(ethylene oxide) and the oligomeric tetraethylene glycol (TEG) and its dimethyl ether derivative (TEGDME) have been reported[23]. The speciation in CH_3-capped oligomer is similar to that present in PPO 3000 triol. By varying the Zn/Br ratio, the speciation can be changed. The $ZnBr_3^-$ species is favoured in the –OH capped oligomers and equations based on competing equilibria have been proposed[23]. The coordination of zinc bromide species with ether oxygens were schematically represented as

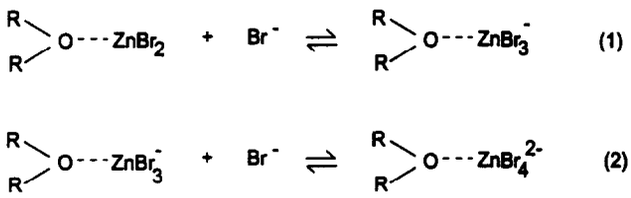

and the Zn–O coordination number would vary depending on the nature of the zinc bromide species. However in the presence of OH-capped polymers, the existence of additional competitive equilibria have been postulated

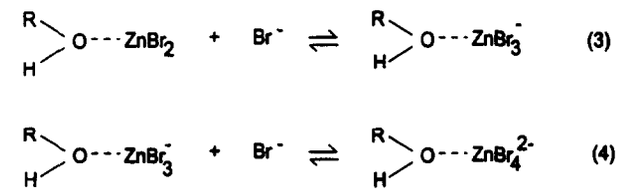

A strong specific interaction of the OH group with the $ZnBr_3^-$ species is suggested. Equilibrium (3) lies to the right while (4) lies to the left.

The effect of adding TEGDME and TEG as plasticizers to $(PEO)_n[(ZnBr_2)_{1-x}(LiBr)_x]$ ($n = 20$, 40; $x = 0$, 0.4, 0.8) also has been studied using Raman spectroscopy. Here, the results are reported for only (PEO + Plasticizer)$_{20}[(ZnBr_2)_{0.2}(LiBr)_{0.8}]$ where 3/1 and 1/1 PEO to plasticizer ratio were used. With the addition of both TEGDME and TEG, the peak at 179 cm^{-1} starts to appear and grows in intensity (see *Table 2* and *Figure 3*). However, the percentage increase of the $ZnBr_3^-$ species relative to $ZnBr_4^{2-}$ is greater for TEG than for the TEGDME-plasticized system, at the same PEO to plasticizer ratio. This fact argues strongly in favour of the presence of the competing equilibria when the –OH end group is present as presented in equations (3) and (4).

The Raman spectra of $(PEO)_n[(ZnBr_2)_{0.2}(LiBr)_{0.8}]$ ($n = 5$, 10, 20) in the region 880–820 cm^{-1} are characterized by peaks at 866, 859 and 844 cm^{-1} (spectra not shown). According to Yoshihara *et al.*[30], the Raman peak at 859 cm^{-1} has been assigned to a mixture of

Table 2 Results of curve-fitting from Raman and EXAFS data

Composition	Relative intensity			Coordination number		R (Å)		D–W factor (Å²)	
	$ZnBr_2$	$ZnBr_3^-$	$ZnBr_4^{2-}$	Zn–Br	Zn–O	Zn–Br	Zn–O	Zn–Br	Zn–O
$(PEO)_{40}ZnBr_2$	70.5	29.5		2.30	3.9	2.34	1.96	5.2E-03	3.8E-02
$(PEO)_{40}[(ZnBr_2)_{0.6}(LiBr)_{0.4}]$	–	89.8	10.2	3.10	2.1	2.39	1.97	5.8E-03	3.2E-02
$(PEO)_{20}[(ZnBr_2)_{0.2}(LiBr)_{0.8}]$			100.0	4.00		2.42	–	6.0E-03	
$(3PEO + TEGDME)_{20}[(ZnBr_2)_{0.2}(LiBr)_{0.8}]$		4.6	95.4	3.95	0.25	2.42	1.96	5.6E-03	2.2E-02
$(PEO + TEGDME)_{20}[(ZnBr_2)_{0.2}(LiBr)_{0.8}]$		23.2	76.8	3.77	0.72	2.42	1.96	5.6E-03	3.0E-02
$(3PEO + TEG)_{20}[(ZnBr_2)_{0.2}(LiBr)_{0.8}]$		20.9	79.1	3.79	0.98	2.42	1.96	6.0E-03	1.8E-02
$(PEO + TEG)_{20}[(ZnBr_2)_{0.2}(LiBr)_{0.8}]$		50.2	49.8	3.50		No EXAFS measurement			

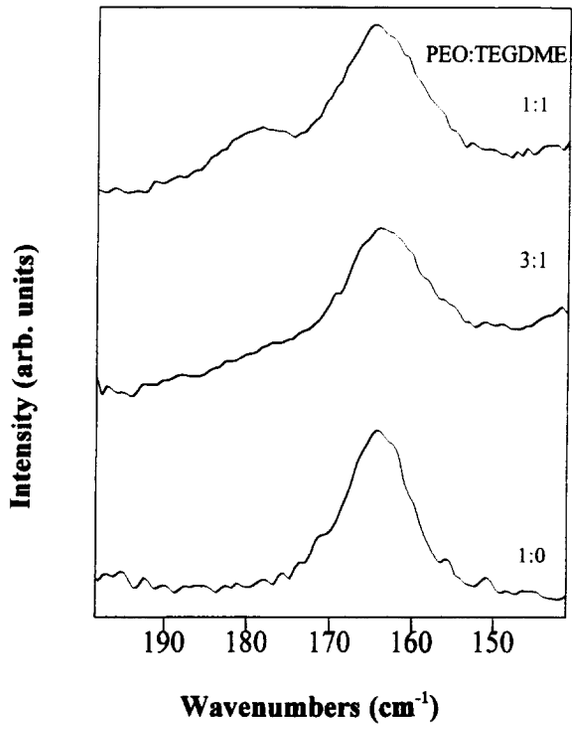

Figure 3 Raman spectra of $(PEO + TEGDME)_{20}[(ZnBr_2)_{0.2}(LiBr)_{0.8}]$ complexes at different PEO:TEGDME ratios in the region 250–140 cm^{-1}

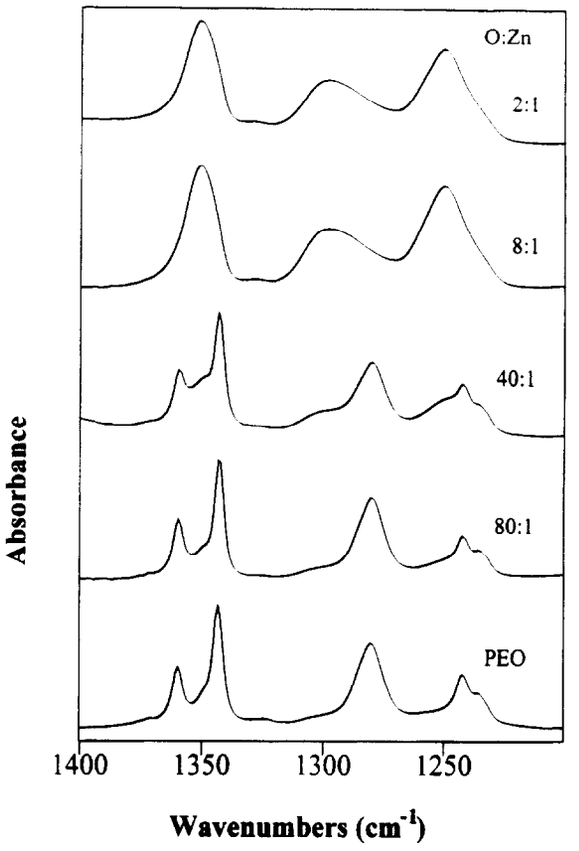

Figure 4 I.r. spectra of $(PEO)_nZnBr_2$ complexes as a function of O:M ratio in the spectral region 1400–1200 cm^{-1}

$r(CH_2)_s$ and $\nu(COC)_s$ in PEO while the band at 844 cm^{-1} has been attributed to $r(CH_2)_a$. With the addition of salt, a shoulder starts growing in at ~866 cm^{-1} and can be ascribed to the wrapping of PEO around Li^+. This peak grows in intensity with an increase in total salt concentration and is also evident in the spectra of $(PEO)_n[(ZnBr_2)_{0.5}(LiBr)_{0.5}]$ ($n = 5$, 10). This observation suggests that the Li^+ ions are wrapped by the PEO chain. This assignment is supported by the Raman study on the PEO–$LiCF_3SO_3$ system[31] where a peak observed at ~867 cm^{-1} has been assigned to the PEO–Li^+ coordination by analogy with *ab initio* calculations of Li^+ in monoethylene glycol dimethyl ether[32]. The peak at 867 cm^{-1} was also observed in the $(TEGDME)_{20}[(ZnBr_2)_{1-x}(LiBr)_x]$ ($x = 0.5$, 0.8) complexes. For the $(PEO)_n[(ZnBr_2)_{0.2}(LiBr)_{0.8}]$ complex, with increasing salt concentration or decreasing n, the relative intensity of the peak at 866 cm^{-1} increases. The trend in intensity variation of the 866 cm^{-1} peak is consistent with the nature of the ionic species present as deduced from bands in the spectral region 250–150 cm^{-1}. The Li^+ being wrapped by PEO serves as a driving force for the preferential formation of $ZnBr_4^{2-}$ and hence the equilibrium [equation (2)] shifts to the right.

Infrared spectroscopy

Figure 4 shows the i.r. spectra of $(PEO)_nZnBr_2$ complexes as a function of concentration in the region 1400–1200 cm^{-1}. The doublet pattern at 1343 and 1360 cm^{-1} due to the CH_2-wag of crystalline PEO[30,33,34] coalesces into a single broad peak at 1352 cm^{-1} which is characteristic for amorphous PEO (the growth of the broad peak is obvious in the 40/1 complex). The peaks at 1278, 1240 and 1234 cm^{-1} correspond to the CH_2 twisting modes. With increasing salt concentration, the peaks are replaced by two broader

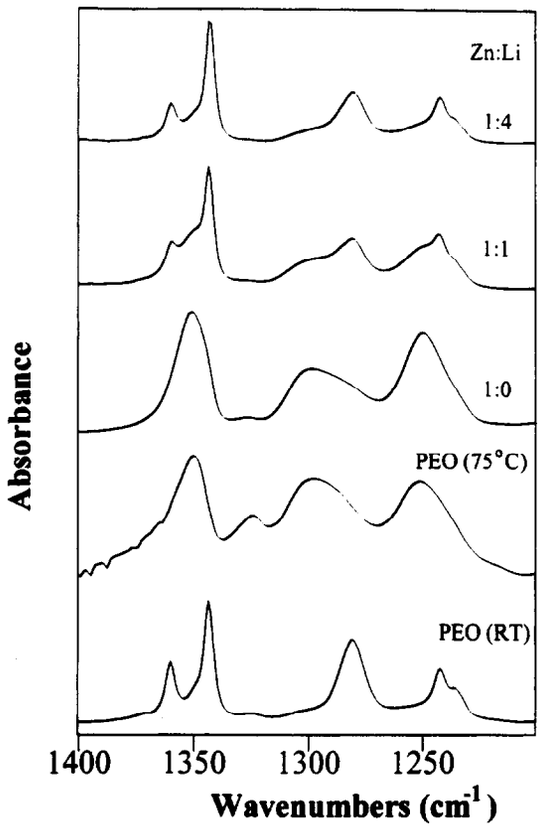

Figure 5 I.r. spectra of $(PEO)_{20}[(ZnBr_2)_{1-x}(LiBr)_x]$ complexes as a function of Zn : Li ratio in the region 1400–1200 cm^{-1}. The spectra of pure PEO at room temperature and 0°C have been included for comparison

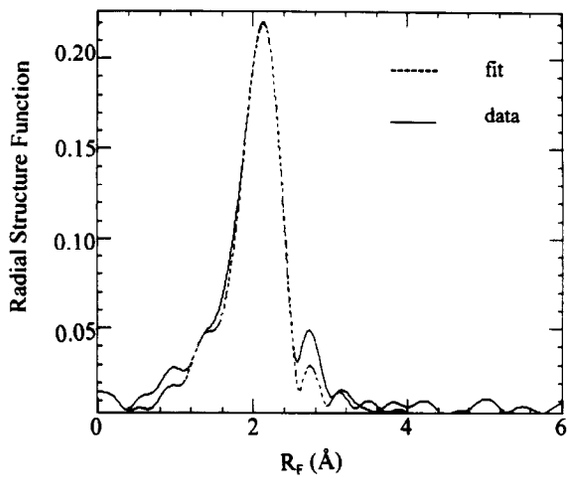

Figure 6 Radial structure function for $(PEO)_{20}[(ZnBr_2)_{0.2}(LiBr)_{0.8}]$

bands at 1302 and 1249 cm^{-1} which are due to amorphous PEO. In the spectral region 1200–1000 cm^{-1} (spectra not shown) three bands at 1153, 1112 and 1058 cm^{-1} which have been assigned to COC symmetric and antisymmetric stretching modes[30,33] are replaced by a single broad peak with the maximum between 1100 and 1000 cm^{-1} at high salt concentrations. Bands in the 1000–800 cm^{-1} region, characteristic of PEO conformation, are all broad at concentrations greater than 20/1. A stacked plot of $(PEO)_{20}ZnBr_2$, $(PEO)_{20}[(ZnBr_2)_{0.5}(LiBr)_{0.5}]$, $(PEO)_{20}[(ZnBr_2)_{0.2}(LiBr)_{0.8}]$, all at room temperatures, and PEO at room temperature and 75°C is shown in *Figure 5*. At an O/M ratio of 20/1,

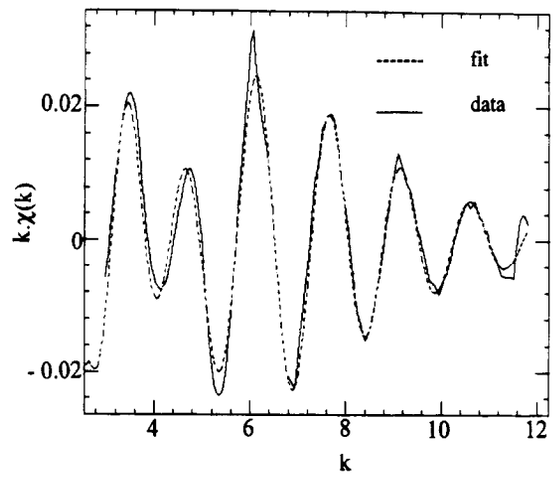

Figure 7 Plot of $k\chi(k)$ vs. k for $(PEO)_{20}[(ZnBr_2)_{0.2}(LiBr)_{0.8}]$

the Zn-rich complexes are more amorphous although a crystalline fraction can be seen in the Zn/Li 1/1 and 1/4 complexes. However, at higher salt concentrations all $(PEO)_n[(ZnBr_2)_{1-x}(LiBr))_x]$ complexes appear to be completely amorphous.

EXAFS

The radial structure function for the composition $(PEO)_{20}[(ZnBr_2)_{0.2}(LiBr)_{0.8}]$ shown in *Figure 6* consists of only a Zn–Br shell. *Figure 7* shows a plot of $k\chi(k)$ vs. k for the same composition. Fits were obtained in k and r spaces with an R-factor of less than 0.02, which indicates excellent agreement between theory and experiment[35]. Inclusion of the second shells of ZnO and $ZnBr_2$ did not improve the fits. The reason for the presence of the side band centered at $R_F \sim 2.8$ in the radial structure function is not known. The absence of a Zn–O contribution in $(PEO)_{20}[(ZnBr_2)_{0.2}(LiBr)_{0.8}]$ suggests that zinc is not coordinated to the ether oxygens. Similar results have been reported by Linford *et al.*[17] for the PEO–Zn/Ca bromide system wherein the species present are $ZnBr_4^{2-}$ and Ca^{2+}, the latter being strongly co-ordinated with up to 12 oxygens from the polymer backbone. For the $(PEO)_{40}ZnBr_2$ and $(PEO)_{40}[(ZnBr_2)_{0.6}(LiBr)_{0.4}]$ systems, the EXAFS data were fit using both Zn–Br and Zn–O coordination shells. The best-fit results for the experimental EXAFS data are shown in *Table 2*. The Zn–Br distances for $(PEO)_{40}ZnBr_2$, $(PEO)_{40}[(ZnBr_2)_{0.6}(LiBr)_{0.4}]$ and $(PEO)_{20}[(ZnBr_2)_{0.2}(LiBr)_{0.8}]$ are 2.34 Å, 2.39 Å and 2.42 Å, respectively. It may be recalled from the Raman data analysis that the former two complexes consist of a mixture of species while only $ZnBr_4^{2-}$ species are present in the third complex. Thus the Zn–Br distance becomes longer with increasing coordination number from 2 to 4. This increase in the Zn–Br distance results from the accommodation of a larger number of Br^- anions around Zn^{2+} in a stable favourable geometry.

The values for the Zn–O coordination numbers obtained from these fits were found to be 7.1 and 5.3 for $(PEO)_{40}ZnBr_2$ and $(PEO)_{40}[(ZnBr_2)_{0.6}(LiBr)_{0.4}]$, respectively. Such high oxygen coordination numbers have been reported by Mendolia and Farrington[36] from their EXAFS studies of PEO–cobalt bromide complexes. They have suggested that owing to the stability of the five-membered chelate ring of the bidentate

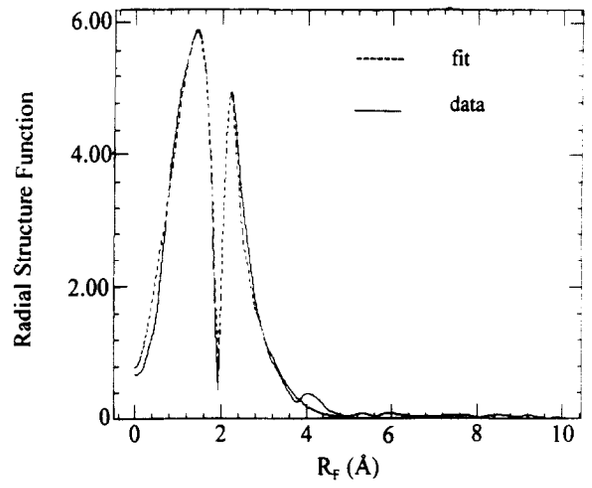

Figure 8 Radial structure function for $(PEO)_{40}[(ZnBr_2)_{0.6}(LiBr)_{0.4}]$

Table 3 Variation of D–W factor for the Zn–Br shell with temperature

Temperature (K)	D–W factor (Å^2)
5.5	0.0024
20.0	0.0024
60.0	0.0025
120.0	0.0031
200.0	0.0048
298.0	0.0060

$-OCH_2CH_2O-$ ligand, $CoBr_3^-$ in PEO must be coordinated with one $-OCH_2CH_2O-$ unit to form a pseudo-tetrahedral complex, in which three Br^- ions take up three apices of the tetrahedron and the two adjacent ether oxygens of the $-OCH_2CH_2O-$ unit take up the remaining tetrahedral position. They also speculated that Co in polyethylene glycol could be complexed with as many as five $-OCH_2CH_2O-$ chelate rings, giving a total oxygen coordination of 10. A similar pseudo-tetrahedral complex of undissociated $CoBr_2$, would be coordinated to a total of two $-OCH_2CH_2O-$ units, or four oxygens. The corresponding octahedral complex would have four $-OCH_2CH_2O-$ units or eight oxygens.

According to the Raman data, Zn–Br coordination numbers of 3.1 and 2.3 were obtained for $(PEO)_{40}[(ZnBr_2)_{0.6}(LiBr)_{0.4}]$ and $(PEO)_{40}ZnBr_2$ respectively. Based on the model presented in the previous paragraph, if zinc is pseudo-tetrahedrally coordinated to Br^- and $-OCH_2CH_2O-$ ligands, then Zn should be coordinated to roughly two and four oxygen atoms respectively. These coordination numbers are very different from the values five and seven actually found for a k-weighting of 1. Further, due to space-filling considerations it is difficult to envisage about five or seven oxygen neighbours in addition to two or three Br^- neighbours around zinc. Upon further examination, it became clear that our conclusion of five to seven oxygen atoms around zinc may have been a result of the inherent error in our data coupled with the k-weighting scheme used. $k = 1$ weighting emphasizes the contribution of bromine atoms in the RSF so that changes in oxygen coordination number are not prominent in the radial structure function. For example, the change in coordination number when the number of oxygen atoms was decreased from 5–7 to 2–4 was less than 5% when $k = 1$ weighting was used. In order to address this problem, a weighting of $k = -1$ was employed so as to emphasize the low k-space data which in turn emphasizes the Zn–O contribution. The radial structure function for $(PEO)_{40}[(ZnBr_2)_{0.6}(LiBr)_{0.4}]$ at a weighting of $k = -1$ is shown in *Figure 8*. Good fits could be obtained and the results are included in *Table 2*. Zn–O coordination numbers of 2.1 for $(PEO)_{40}[(ZnBr_2)_{0.6}(LiBr)_{0.4}]$ and 3.9 for $(PEO)_{40}ZnBr_2$ were obtained. When values of five and seven were used for Zn–O coordination numbers at $k = -1$ weighting, it was observed that the fits worsened by about 30%. Zn–O coordination numbers of 2.1 for $(PEO)_{40}[(ZnBr_2)_{0.6}(LiBr)_{0.4}]$ and 3.9 for $(PEO)_{40}ZnBr_2$ can be reasonably explained along the ideas suggested by Mendolia and Farrington[36]. The Zn–O distances obtained for the two complexes are 1.96 Å and 1.97 Å respectively which are identical within experimental error. This result is surprising, since in simple zinc compounds with only oxygen in the first shell, the Zn–O distance scales with the number of oxygen atoms in the first shell[37]. The high Debye–Waller factors for the Zn–O shell suggest that either the oxygen atoms exist at more than one distance and these distances are widely separated (on the order of 0.15–0.2 Å) or the oxygen atoms are weakly coordinated to the zinc atom and hence thermal vibrations are quite large. Low temperature EXAFS studies would allow us to distinguish between these two possibilities; these studies are planned for the future.

A temperature variation EXAFS study was carried out on the $(PEO)_{20}[(ZnBr_2)_{0.2}(LiBr)_{0.8}]$ sample at 5.5 K, 20 K, 60 K, 120 K and 200 K and room temperature. In this complex only the $ZnBr_4^{2-}$ species was observed in the Raman data. The EXAFS data could be fit to the Zn–Br coordination shell. The Zn–Br coordination number and distance did not change and a Zn–O contribution was not observed on lowering the temperature. The effect of temperature on the speciation in these types of systems has been studied before in the literature, and the results are mixed. Linford *et al.*[14] studied the PEO_4ZnBr_2 complex at room temperature and −70°C. They reported that the Zn–O distance did change as a function of temperature while the Zn–Br distance did not and suggested the presence of neutral $ZnBr_2$ species. However, a similar study on $(PEO)_{16}ZnBr_2$ by McBreen *et al.*[15] showed a decrease in Zn–Br coordination number from 1.8 to 1.54 and a corresponding decrease in distance of 0.01 Å, in going from 25 to 120°C, which the authors attributed to a change in speciation. However, a temperature variation Raman study of PPO–$ZnBr_2$ salt complexes in the range 25–100°C showed no significant change in the zinc bromide speciation[23].

Table 3 summarizes the temperature dependence of the Zn–Br D–W factor for the $(PEO)_{20}[(ZnBr_2)_{0.2}(LiBr)_{0.8}]$ complex. At very low temperatures the D–W factor is 0.0024 Å^2 and increases gradually with increase in temperature. The D–W factor consists of a thermal term and a disorder term. The former diminishes with decreasing temperature, whereas the disorder term is either constant or may even increase at low temperatures. Based on their EXAFS study of the $(PEO)_4ZnBr_2$ complex, Linford *et al.*[14] did not note an obvious trend towards a reduction in the D–W factors as the temperature is decreased over the range of room temperature to −70°C and suggested that the

disorder term predominates. However, the data in this study are presented for a much wider range of temperatures and show an obvious decrease in the D–W factor with a decrease in temperature. This decrease clearly indicates a significant contribution from the thermal term towards the D–W factor at room temperature.

The effect of addition of plasticizers was studied by EXAFS. For the complexes $(PEO + P)_{20}$-$[(ZnBr_2)_{0.2}(LiBr)_{0.8}]$ (P = TEGDME, TEG), the Zn–O shell was included in the fitting procedure. The results are included in *Table 2*. The Zn–O contribution, although small, increased with increasing plasticizer content; the result is consistent with the Raman data. The addition of plasticizer leads to the formation of $ZnBr_3^-$ species and hence the Zn–O contribution becomes significant. The results also show that the Zn–O contribution is greater when TEG is used as a plasticizer compared to TEGDME, at the same mol%; again consistent with the Raman results. The effect of end-group on speciation is emphasized and can be rationalized on the basis of the competing equilibria described earlier. A similar observation regarding end-group effect was made by Linford *et al.* based on their plasticizer study in the $(PEO)_nNiBr_2$ system[29].

CONCLUSIONS

Raman spectroscopic data in the $(PEO)_n$-$[(ZnBr_2)_{1-x}(LiBr)_x]$ complexes reveal that the zinc bromide species change from $ZnBr_2$ to $ZnBr_3^-$ to $ZnBr_4^{2-}$ when x is varied from 0 to 0.8 at a constant O : M ratio. Similarly the speciation also changes when n is varied with x being constant. EXAFS results indicate no Zn–O coordination for $(PEO)_{20}[(ZnBr_2)_{0.2}(LiBr)_{0.8}]$ while Zn–O coordination numbers of 2.1 and 3.9 respectively are obtained for $(PEO)_{40}[(ZnBr_2)_{0.6}(LiBr)_{0.4}]$ and $(PEO)_{40}ZnBr_2$. With addition of TEG and TEGDME to $(PEO)_{20}[(ZnBr_2)_{0.2}(LiBr)_{0.8}]$, the Raman and EXAFS data show the presence of $ZnBr_3^-$ species and a corresponding increase in the Zn–O coordination number. The results from Br K-edge EXAFS spectra indicate that each Br has only one Zn neighbour. Similar results have been reported by Neat *et al.*[38] from Br *K*-edge EXAFS studies. The zinc–bromine distances are substantially less than the sum of the appropriate ionic radii thereby suggesting that the zinc–bromide species present have some covalent character. A temperature dependent EXAFS study shows that speciation seems relatively unaffected by cooling to below the glass transition temperature for $(PEO)_{20}[(ZnBr_2)_{0.2}(LiBr)_{0.8}]$ which only has Zn–Br coordination at room temperature. A Zn–O contribution was absent even at very low temperatures.

ACKNOWLEDGEMENTS

The authors would like to thank Berlin Genetti for his assistance in collection of data at SSRL and the SSRL staff, in particular Britt Hedman and Ingrid Pickering. The authors would also like to thank Dr Matthew Newville for his advice regarding the k weighting parameters. This work has been supported by funds from the U.S. Army Research Office (Grant No. DAAH04-94-G-0250) and from the NSF EPSCoR program (Cooperative agreement No. OSR-9550478).

REFERENCES

1. Armand, M. B., Chabagno, J. M. and Duclot, M., in *Fast Ion Transport in Solids*, ed. P. Vashista, J. N. Mundy and G. K. Shenoy. Elsevier Applied Science, North Holland and New York, 1979, p. 131.
2. Scrosati, B., in *Applications of Electroactive Polymers*, ed. B. Scrosati. Chapman and Hall, London, 1993, p. 251.
3. Gray, F. M., *Solid Polymer Electrolytes: Fundamentals and Technological Applications*. VCH, New York, 1991.
4. Hagan, W. P., Latham, R. J., Linford, R. G. and Vickers, S. L., *Solid State Ionics*, 1994, **70–71**, 666.
5. Fauteux, D., Massucco, A., Mclin, M., van Buren, M. and Shi, J., *Electrochim. Acta*, 1995, **40**, 2185.
6. Hooper, A., Gauthier, M. and Belanger, A., in *Electrochemical Science and Technology of Polymers*, ed. R. G. Linford, Vol. 2. Elsevier Applied Science, London, 1990, p. 375.
7. Armand, M. B., in *Polymer Electrolyte Reviews*, ed. J. R. MacCallum and C. A. Vincent, Vol. 1. Elsevier Applied Science, London, 1989, p. 1.
8. Berthier, C., Gorecki, W., Minier, M., Armand, M. B., Chabagno, J. M. and Rigaud, P., *Solid State Ionics*, 1983, **11**, 91.
9. Fauteux, D., Prud' homme, J. and Harvey, P. E., *Solid State Ionics*, 1988, **28–30**, 923.
10. Stern, E. A., in *X-ray Absorption Principles, Applications, Techniques of EXAFS, SEXAFS and XANES*, ed. D. C. Koninsberger and R. Prins. Wiley-Interscience, New York, 1988, p. 3.
11. Yang, H. and Farrington, G. C., *J. Electrochem. Soc.*, 1992, **139**, 1646.
12. Yang, H. and Farrington, G. C., *J. Polym. Sci. Polym. Phys. Ed.*, 1993, **31**, 157.
13. Yang, H., Huq, R. and Farrington, G. C., *Solid State Ionics*, 1990, **40/41**, 663.
14. Glasse, M. D., Latham, R. J., Linford, R. G. and Pynenburg, R. A. J., *Solid State Ionics*, 1992, **53–56**, 1111.
15. McBreen, J. and Lin, I.-C., *J. Electrochem. Soc.*, 1992, **139**, 960.
16. Linford, R. G., *Faraday Discuss. Chem. Soc.*, 1989, **88**, 133.
17. Latham, R. J., Linford, R. G., Pynenburg, R. and Schlindwein, W. S., *Electrochim. Acta*, 1992, **37**, 1529.
18. Sheldon, M. H., Glasse, M. D., Latham, R. J. and Linford, R. G., *Solid State Ionics*, 1989, **34**, 135.
19. Chowdhari, B. V. R., Huq, R. and Farrington, G. C., *Electrochim. Acta*, 1992, **37**, 1667.
20. Latham, R. J., Linford, R. G. and Schlindwein, W. S., *Faraday Discuss. Chem. Soc.*, 1989, **99**, 103.
21. Farrington, G. C. and Linford, R. G., in *Polymer Electrolyte Reviews*, ed. J. R. MacCallum and C. A. Vincent, Vol. 2. Elsevier, London, 1989.
22. Chowdhari, B. V. R., Huq, R. and Farrington, G. C., *Solid State Ionics*, 1992, **57**, 49.
23. Chintapalli, S. and Frech, R., *Electrochim. Acta*, 1995, **40**, 2093.
24. Rehr, J. J., Zabinsky, S. I. and Albers, R. C., *Phys. Rev. Lett.*, 1992, **69**, 3397.
25. Teo, B. K., in *EXAFS: Basic Principles and Data Analysis*, Ch. 5. Springer-Verlag, New York, 1986.
26. Yellin, W. and Plane, R. A., *J. Am. Chem. Soc.*, 1961, **83**, 2448.
27. Macklin, J. W. and Plane, R. A., *Inorg. Chem.*, 1970, **9**, 821.
28. Morris, D. F. C., Short, E. L. and Waters, D. N., *J. Inorg. Nucl. Chem.*, 1963, **25**, 975.
29. Latham, R. J., Linford, R. G., Pynenburg, R. A. J. and Schlindwein, W. S., *J. Chem. Soc. Faraday Trans.*, 1993, **89**, 349.
30. Yoshihara, T., Tadokoro, H. and Murahashi, S., *J. Chem. Phys.*, 1964, **41**, 2902.
31. Dissanayake, M. A. K. L. and Frech, R., *Macromolecules*, 1995, **29**, 5312.
32. Huang, W., Frech, R. and Wheeler, R. A., *J. Phys. Chem.*, 1994, **98**, 100.
33. Papke, B. L., Ratner, M. A. and Shriver, D. F., *J. Phys. Chem. Solids*, 1981, **42**, 493.
34. Li, X. and Hsu, S. L., *J. Polym. Sci. Polym. Phys.*, 1984, **22**, 1331.
35. Newville, M., private communication.
36. Mendolia, M. S. and Farrington, G. C., *Electrochim. Acta*, 1992, **37**, 1695.
37. Pan, H. K., Knapp, G. S. and Cooper, S. L., *Colloid and Polymer Sci.*, 1984, **262**, 734.
38. Neat, R. J., Glasse, M. D., Linford, R. G. and Hooper, A., *Solid State Ionics*, 1986, **18/19**, 1088.